29 March 1985, Volume 227, Number 4694 SCIENCE

High-Resolution Nuclear Magnetic Resonance of Inorganic Solids

Eric Oldfield and R. James Kirkpatrick

Summary. Recent improvements in instrumentation and technique now permit the observation of high-resolution nuclear magnetic resonance spectra of many nuclei in inorganic solids. The application of nuclear magnetic resonance to the study of the structures of materials of interest in chemistry, earth science, and materials science are discussed together with a prognosis for future work.

During the past 3 years there has been increased interest in applying high-resolution solid-state nuclear magnetic resonance (NMR) spectroscopy to the study of inorganic solids such as minerals and heterogeneous catalysts (*1, 2*). This increased activity has been primarily brought about by the commercial availability of sensitive Fourier-transform NMR spectrometers with superconducting magnets. In addition, NMR techniques for observing, in solids, nuclei with both spin $I = 1/2$ and spin $I = 3/2$, 5/2, 7/2, and 9/2 (quadrupolar nuclei) have been developed (*3–8*). In the next few years, such techniques will have a major impact on geochemistry, materials research, and heterogeneous catalysis; and solid-state NMR spectroscopy will become as routine a tool in these inorganic areas as liquid-state NMR has been in other areas of chemistry over the past 20 years.

In geochemistry, the nucleus that is the most desirable candidate for NMR studies is oxygen, since it constitutes 62.5 percent of the earth's crust. Unfortunately, its only NMR-active nuclide is ^{17}O. Oxygen-17 has a 0.037 percent natural abundance and a quadrupole moment of 2.6×10^{-30} m^2, which together give rise to broad and weak spectral lines. Silicon, 21.2 percent of the earth's crust, and aluminum, 6.5 percent, are the next most abundant elements. Aluminum-27 has a 100 percent natural abundance, resulting in a strong resonance, although its low quadrupole moment, 0.149×10^{-28} m^2, makes the resonance broad. Silicon-29 has only a 4.7 percent natural abundance; but it has a nuclear spin, I, of 1/2, so it gives sharp spectral lines. Thus, early research on the NMR spectra of geochemically and catalytically interesting solids has been confined to ^{27}Al and ^{29}Si (*1–4*).

Eric Oldfield is a professor of chemistry and R. James Kirkpatrick is a professor of geology at the University of Illinois, Urbana 61801.

Theory and Experiment

Figure 1a shows a nuclear energy level diagram for ^{29}Si, $I = 1/2$, in a strong magnetic field; Fig. 1b, a typical spectral line shape for a stationary ^{29}Si NMR sample; and Fig. 1c, a ^{29}Si NMR spectrum obtained from a rapidly rotated crystalline silicate [obtained at 71.5 MHz, corresponding to a magnetic field strength of 8.45 Tesla (T) or a ^1H-resonance frequency of 360 MHz].

When ^{29}Si is placed in a strong magnetic field, the energy levels with $I = 1/2$ and $-1/2$ have their degeneracy lifted, and transitions between the levels may be detected in the NMR experiment. In the absence of any other interaction, this gives rise to a sharp resonance at some frequency, ω_0. However, a number of orientation-dependent interactions perturb these energy levels and result in line broadening. For example, in the sheet silicate $Na_2Si_2O_5$, the NMR resonance frequency of ^{29}Si (its chemical shift) is strongly dependent on the spatial orientation of the silicate group because of the nonspherical electron distribution around the silicon nucleus. This leads to a broad spectral line (Fig. 1b) whose breadth and shape are determined by a chemical-shielding tensor. Dipolar interactions between the nuclear spins and, for nuclei having $I \geq 1$, quadrupolar interactions between the nuclear quadrupole moment (eQ) and the electric field gradient (eq) at the nucleus may cause further spectral broadening.

All of these interactions lead to decreased spectral resolution and low ratios of signal to noise. For years they impeded the use of NMR for studying the structures of most inorganic solids. Fortunately, it was shown that each of these second-rank tensor interactions may be eliminated by rapid mechanical rotation of the sample at a unique angle to the main magnetic field, the "magic angle," $\theta = 54.7°$. If the sample rotation rate, when expressed in frequency units, is much greater than the spectral broadening, the mathematical term $3\cos^2\theta - 1$ that appears in the time-average values of these interactions vanishes (*9–12*). Under these conditions, scalar couplings (*13*), isotropic chemical shifts, and Knight shifts (*14, 15*) may be observed. This technique is called magic-angle sample-spinning (MASS) NMR.

With less rapid rotation, well-resolved spinning sidebands form about the isotropic centerband at multiples of the spinning frequency (ω_r). For the anisotropic chemical-shift interactions or Knight-shift interactions, these sidebands may be considered a mechanical echo in the time domain after one rotor revolution (*16*). Figure 1c shows a typical result for the chemical shift anisotropy of ^{29}Si in $Na_2Si_2O_5$.

In the experiment, samples of a few hundred milligrams are rotated on air bearings at frequencies of up to 5 kHz (~300,000 rpm). A typical rotor design and the orientation of the axis of rotation in the magnetic field is shown in Fig. 1d (*11*). The materials used for such rotor assemblies are chosen to provide low background signals from an empty probe. They typically include plastics

such as Delrin or Kel-F and inorganics and ceramics such as sapphire, BN, and Macor. With appropriate design, both solid-packed and vacuum-sealed samples can be studied, and sample temperatures from ~5 K to ~500 K are accessible.

Silicon-29 NMR

Silicon was the first inorganic element to be studied in a variety of catalyst and mineral samples (*1–3*). Silicon-29 resonates at 39.7 MHz in a 4.7 T magnetic field (corresponding to a ^{1}H-resonance frequency of 200 MHz). Because there is no associated quadrupole moment, the absorption lines are quite narrow and the sensitivity is high. Indeed, very early investigation by Holzman *et al.* (*17*) indicated considerable promise for high-resolution, solid-state NMR of silicon. However, it was only after the advent of commercial, high-field Fourier-transform NMR spectrometers some 20 years later that the promise was realized.

The results obtained to date show that NMR has great potential for investigating the structures of amorphous phases—glasses and various fine-grained materials such as clays and zeolites—that cannot be readily investigated by means of single-crystal diffraction techniques. Quantitative information on the type of sites present and the order or disorder at a given site may usually be obtained in short time periods (minutes to a few hours). The data obtained—chemical shifts, chemical-shielding tensors, and, for quadrupolar nuclei, electric-field-gradient tensors—can be interpreted in terms of types of chemical bonding—covalency, bond angles, and bond distances. Moreover, in many cases, NMR may be used to determine the rates of motion of the various species present.

In Fig. 2 we show ^{29}Si spectra that illustrate the points discussed above. For example, in Fig. 2a we show ^{29}Si NMR spectra of diopside ($CaMgSi_2O_6$), clinoenstatite ($MgSiO_3$), and α-silicon carbide (SiC). From x-ray crystallography, we know diopside has only one silicon site, whereas clinoenstatite has two (*18, 19*). The ^{29}Si NMR spectra indeed show one center band resonance for diopside (at −84 ppm from an external sample of tetramethylsilane), but two peaks for enstatite, at −81 and −83 ppm (*20*). The spinning sidebands, which are marked with an asterisk for both samples, are due to the presence of a large chemical shift anisotropy. For α-SiC there are three peaks—a rather unexpected result due, perhaps, to the polytypic nature of this sample.

For the silicate minerals, the ranges of isotropic chemical shifts are a function of the different states of polymerization of the SiO_4 tetrahedra (Q^0, Q^1, Q^2, Q^3, and Q^4). This makes ^{29}Si NMR a most useful structure-sensitive tool.

Aluminum in framework (Q^4) silicates, such as feldspar minerals and synthetic zeolites, causes a systematic deshielding at ^{29}Si (corresponding to so-called low-field, high-frequency, or paramagnetic shifts). For example, in the zeolite Linde A, there is only one silicon resonance (at about −88.5 ppm, depending on the counterions present), corresponding to Si(4Al), in accord with a framework Si:Al ratio of 1.0 and obeyance of Loewenstein's rule (*21, 22*). For Linde Y, there are a series of peaks, corresponding to Si(1Al) through Si(4Al) (*23*), as shown in Fig. 2b. Analysis of the relative integrated peak intensities for Linde Y yields the ratio of silicon to aluminum in the framework. That value is difficult to obtain by other analytical methods owing to the frequent occurrence of extra-framework aluminum, which may be directly detected by ^{27}Al NMR.

The silicon spectra shown in Fig. 2, a and b, are from materials that are fairly well-defined crystallographically. In contrast, Fig. 2c shows the ^{29}Si MASS NMR spectrum of a sample of shocked sandstone from Meteor Crater, Arizona, together with spectra of quartz (SiO_2) crystal and quartz glass. Our results (*24*) indicate that while much of the SiO_2 in the meteor-crater sample is present as crystalline quartz, as demonstrated by the sharp resonance at −108 ppm, approximately 5 percent is also present as the high-pressure polymorphs stishovite and coesite, as demonstrated by the peaks at −191.1 ppm for stishovite, which contains six-coordinate silicon at-

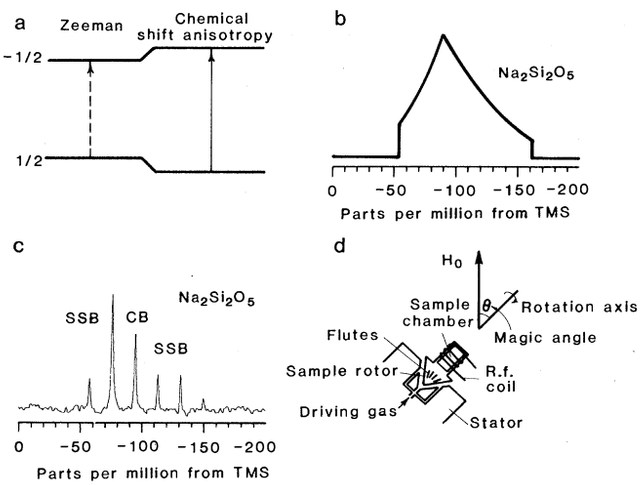

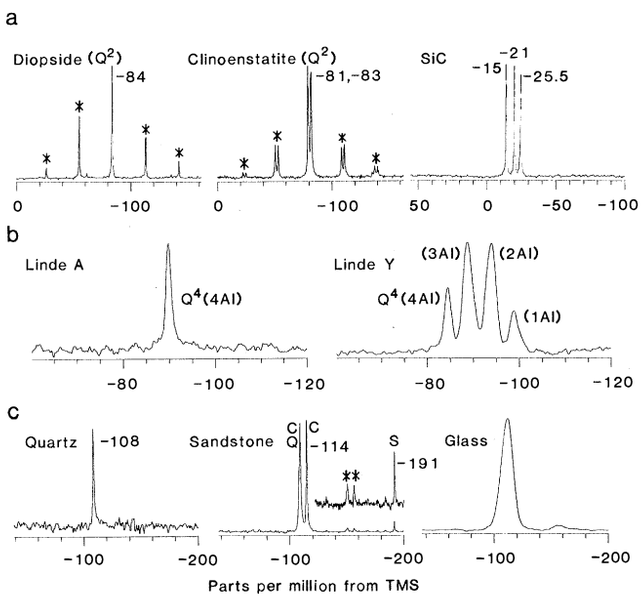

Fig. 1 (left). (a) Energy level diagram for ^{29}Si nucleus (I = 1/2) in a strong magnetic field. The effect of perturbation of the nuclear Zeeman levels due to chemical shielding is illustrated. (b) Powder-pattern line shape due to anisotropic chemical shielding in an NMR spectrum for ^{29}Si in a silicate. (c) High-field (8.45 T) ^{29}Si NMR spectrum of $Na_2Si_2O_5$ obtained by means of magic-angle sample spinning (MASS). Abbreviation: CB, center band; SSB, spinning side bands. (d) Rotation axis of NMR sample with respect to the direct-current and radio-frequency field directions. Fig. 2 (right). Silicon-29 MASS NMR spectra of minerals, zeolites, and a glass. Peaks marked with asterisks are spinning sidebands. (a) Spectra of diopside ($CaMgSi_2O_6$), clinoenstatite ($MgSiO_3$), and silicon carbide (SiC), showing the presence of one silicon site and two and three nonequivalent silicon sites, respectively. (b) Spectrum of Linde A and Linde Y, showing the deshielding effects of aluminum. (c) Spectra of SiO_2 phases: quartz; sandstone from Meteor Crater, Arizona, showing quartz (Q), coesite (C), and stishovite (S) peaks; and glass.

oms (*25*), and −108.1 and −113.9 ppm for coesite, which contains four-coordinate silicon atoms. When long recycle times are used in the experiment (to avoid saturation of the quartz resonance), observation of the stishovite peak is most difficult (*24*). With short recycle times, quantitative analysis of the high-pressure polymorphs in whole-rock samples is quite feasible (*24*). Thus, ^{29}Si MASS NMR should be capable of detecting such species in other mineral samples that have been subjected to intense pressure.

Finally, we also show in Fig. 2c the ^{29}Si spectrum of vitreous SiO_2, prepared by rapidly quenching a SiO_2 melt from about 1850°C. The resonance here is quite broad, and it extends from about −95 to −125 ppm. To date, there have been four main approaches to the analysis of such chemical shift information. First of all, the early studies of Lippmaa *et al.* (*1, 3*) and Fyfe and Thomas and their co-workers (*2*), suggested the presence of nonoverlapping chemical shift ranges, that is, the chemical shift for ^{29}Si nuclei in Q^0 compounds did not overlap with those for ^{29}Si in Q^1 compounds. Such optimistic relations soon broke down as more samples were examined. There is great overlap in the range of isotropic ^{29}Si chemical shifts for silicon sites with different states of polymerization (Q^0 to Q^4) and for framework silicates with one to four aluminum atoms as next-nearest neighbors.

One successful method for interpreting these chemical shifts has been the Brown and Shannon (*26*) bond-strength method (*20, 27*). These bond strengths are similar to the electrostatic bond strengths of Pauling but have been modified to include the effects of interatomic distance. To do this, the cation-oxygen bond strengths for all cations bonded to the four oxygens of a silica tetrahedron are totaled. These "cations" include the silicon atom itself and all cations outside the tetrahedron that are coordinated to these oxygens.

Pauling's original postulate was that the sum of the electrostatic bond strengths of the cations surrounding an oxygen atom should equal the absolute value of the valence of oxygen, where the bond strength for a cation is its valence divided by its coordination number. This rule has been used in evaluating crystal structures determined by x-ray and neutron diffraction. However, the rule does not hold exactly for many structures, and bond lengths increase or decrease to compensate for too much or too little charge (*28*).

The relation between bond strength and chemical shift shown in Fig. 3a offers an explanation for the ranges of chemical shifts for the different structural types observed by Lippmaa *et al.* (*1, 3*), for the overlap of these ranges, and for the deshielding caused by the substitution of aluminum into the silicon sites (*27*).

The sums of the bond strengths for a particular structural type tend to fall into one range, because the average number of silicon atoms bonded to a silicate tetrahedron decreases with decreasing polymerization. Silicon atoms have the largest effect on the ^{29}Si chemical shift, which is understandable since the Si–O bond is the strongest one involved [443 kJ/gram-atom (*29*)]. Variation in the kind and arrangement of other cations within a given structural type, however, causes the ranges in chemical shift to be large enough to overlap. This is especially true if the aluminum is six coordinate, as in the Al_2SiO_5 polymorphs. Substitution of aluminum for silicon in the tetracoordinated sites results in a lower bond-strength sum because the Al–O bond is weaker (330 to 422 kJ/gram-atom) than the Si–O bond, which corresponds with the less negative chemical shift. Bonds to monovalent or divalent cations are even weaker and result in further deshielding. Overall, the observed correlation between chemical shift and the sum of bond strengths is very good (correlation coefficient of 0.88), as shown in Fig. 3a.

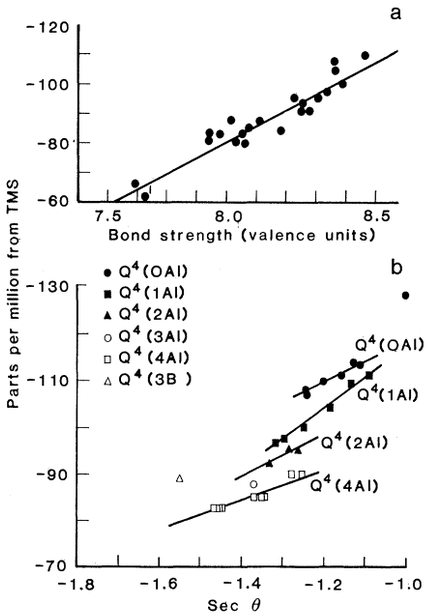

Fig. 3. Analyses of ^{29}Si chemical shifts. (a) A plot of chemical shift as a function of bond strength. (b) A plot of chemical shift as a function of Si–O–Si bond angle, θ, for framework silicates containing zero, one, two, three, and four aluminums per SiO_4 tetrahedron (*30*).

However, when only framework (Q^4) silicates are examined (*30, 31*) an even better chemical-shift correlation may be made with the secant of the Si–O–T (T = Si, Al) bond angle, θ, a relation suggested by the molecular orbital calculations of Gibbs (*32*). We have extended these results to framework silicates containing zero, one, two, and four aluminum atoms per SiO_4 tetrahedron (Fig. 3b), and Ramdas and Klinowski have recently obtained similar excellent correlations based on total Si · · · T nonbonded distances for silicon in the five kinds of Si (or Al) environments (*33*). Figure 3 thus indicates that, for silicates of unknown structure, proposed structural models must be consistent with the observed ^{29}Si chemical shifts; it also shows that, for framework silicates, Si–O–T bond angles may be determined with some accuracy from the NMR observations. Such observations hold considerable promise for the structural analysis of amorphous materials. For example, the broad line shape of the SiO_2 glass in Fig. 2c may be analyzed in terms of various distribution functions of the Si–O–Si bond angles (*34*).

NMR of Quadrupolar Nuclei:

Theory and Background

Most of the nuclei in the Periodic Table have a nuclear spin $I \geq 1$ and thus possess a quadrupole moment, which in most chemical environments leads to extensive line broadening. Fortunately, however, most of these quadrupolar nuclei also have a nonintegral spin (I = 3/2, 5/2, 7/2, or 9/2). As shown in the energy-level diagram for ^{23}Na (I = 3/2) in Fig. 4a, the central transition (1/2 ↔ −1/2) of each such nucleus is unaffected, to first order, by this quadrupole interaction. For ^{23}Na, the first-order quadrupole interaction leads to a static NMR spectrum composed of two broad absorptions due to the satellite transitions (3/2 ↔ 1/2, −1/2 ↔ −3/2) and a sharp central absorption (1/2 ↔ −1/2) broadened only by dipole, chemical-shift, and scalar-coupled interactions (Fig. 4b). In general, with MASS NMR, these interactions are again averaged, and the sharp central absorption is observed together with a number of sidebands due to the satellite transitions (Fig. 4c).

When the quadrupole coupling constant is about 1 MHz, only the central (1/2 ↔ −1/2) resonance is readily detected experimentally, because there is usually significant broadening of the satellite lines due to either small fluctuations around the magic angle caused by rotor

wobble or a slight missetting of the magic angle. In fact, it is sometimes desirable to deliberately misset the magic angle in order to better define the line shape from the central transition. Missetting the magic angle introduces a residual broadening equal to about 2.5 percent of the line width from the solid sample if it were static, per degree of misset. In the case of the ^{51}V NMR spectrum of $NaVO_3$, for example, residual broadening of the first-order satellite lines is nearly two orders of magnitude larger than that of the central ($1/2 \leftrightarrow -1/2$) line, which is broadened by chemical shift anisotropy. This difference in broadening allows an accurate determination of the ^{51}V chemical-shift tensor (*35*), yielding $\sigma_{11} = -213$ ppm, $\sigma_{22} = -56$ ppm, and $\sigma_{33} = 269$ ppm, from an analysis of the sideband intensities (*36*).

When the quadrupole coupling constant is even larger, about 3 to 10 MHz, fine structure appears on the central line, a result of the higher order effects that arise when the quadrupole interaction is a significant fraction of the actual resonance frequency. For example, in Na_2MoO_4 the quadrupole coupling constant for ^{23}Na is approximately 2.6 MHz, and at all fields in the range 3.52 to 11.7 T there is pronounced second-order broadening of the central transition (Fig. 5a). Spinning the sample at the magic angle is only partially effective in removing this broadening (Fig. 5b), because it is described by a more complex angle dependence than the first-order interaction and does not vanish for any rotational angle. There are, however, optimal angles, which depend on the value of the asymmetry parameter of the electric-field-gradient tensor (*6, 37–41*). Figure 5c shows that spinning a sample of $^{23}Na_2MoO_4$ at 75° from the magnetic field gives a resonance line twice as narrow as that obtained at 54.7°. However, dipolar interactions and chemical-shift anisotropy interactions do not vanish under these conditions and can thus cause additional unwanted line broadening.

For most materials, the best initial strategy for studying a quadrupolar nucleus is to perform the experiment at as high a magnetic field strength as possible while spinning the sample at the magic angle (54.7°). This generally provides the best sensitivity and resolution and minimizes the need to correct the chemical shift for the second-order shift (*42, 43*). However, the case where two nuclei, A and B, have the same isotropic chemical shift but different quadrupole coupling constant (e^2qQ/h) is an exception. In a high field, A and B will be unresolvable, whereas in a low field, the second-order quadrupole interaction shifts the resonance with the larger value of e^2qQ/h, permitting its resolution. An example, the case of $^{11}BO_4$ and $^{11}BO_3$ units in a borosilicate glass, is shown in Fig. 5, d and e (*44*). With this information we can now discuss the high-field NMR spectra of a number of quadrupolar nuclei of interest to chemists and earth and materials scientists.

Oxygen-17 NMR Spectra

Oxygen-17 has a nuclear spin $I = 5/2$ and a quadrupole moment of -2.6×10^{-30} m^2, is only 0.037 percent abundant in nature, and resonates at 67.8 MHz in a magnetic field of 11.7 T (500 MHz ^1H-resonance frequency). When it is in sites of less than cubic symmetry, there is thus considerable line broadening in its spectrum due to the quadrupole interaction. This line broadening and the low abundance have, until recently, precluded observation with NMR spectroscopy of this most important element—the most abundant element in the earth's crust.

However, in sites with cubic or close-to-cubic symmetry, ^{17}O MASS NMR lines are very narrow, ~1 ppm (*7, 8*), and spectra may be obtained even at natural abundance (*45–47*). The range of chemical shifts for group IIA oxides spans 618 ppm (*47*), from 22 ppm for BeO to 640 ppm for BaO; and the shifts are a function of the cation electronegativities, as observed in the ^{19}F NMR spectra of the group IA fluorides (*48*). There is also an excellent relation between the ^{17}O chemical shifts and the cation radius (*47*). Furthermore, in some cases, complete powder patterns may be obtained for static samples, yielding accurate values for e^2qQ/h. For example, with ZnO, $e^2qQ/h = 120$ kHz (*47*).

While such results with the group II elements might have been expected, more startling was the observation of

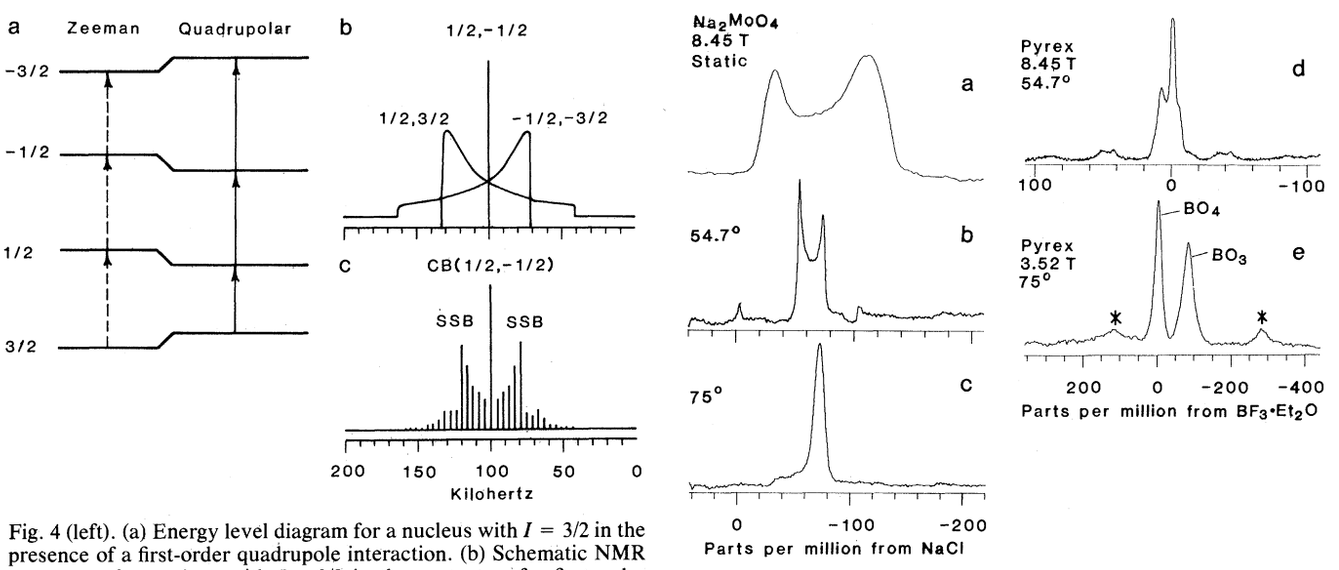

Fig. 4 (left). (a) Energy level diagram for a nucleus with $I = 3/2$ in the presence of a first-order quadrupole interaction. (b) Schematic NMR spectrum of a nucleus with $I = 3/2$ in the presence of a first-order quadrupole interaction. (c) Schematic MASS NMR spectrum of a nucleus with $I = 3/2$ in the presence of a first-order quadrupole interaction. Fig. 5 (right). (a) Line shape of central ($1/2 \leftrightarrow -1/2$) transition of ^{23}Na in Na_2MoO_4 in a static sample at 8.45 T. The effect of second-order broadening ($e^2qQ/h = 2.6$ MHz) can be seen. (b) Sodium-23 MASS NMR spectrum of sample in (a) at 8.45 T. (c) Sodium-23 NMR spectrum of sample in (a) spun at 75° from the applied field at 8.45 T. (d) Boron-11 MASS NMR spectrum of a borosilicate glass at 8.45 T showing poorly resolved BO_3 and BO_4 resonances. (e) NMR spectrum of the sample in (d) spun at 75° from the applied field at 3.52 T. The BO_3 and BO_4 resonances are well resolved due to a significant second-order quadrupole shift of the resonance from trigonal BO_3.

high resolution spectra of complex oxoanions [tungstates, molybdates, and vanadates (*8*)], as well as of ^{17}O in the CO ligands of a number of metal carbonyls (*49*). Such spectra are visible, because the e^2qQ/h values are small, and, thus MASS line widths of only 1 or 2 ppm are obtained at high magnetic field strengths; in many such systems the corresponding chemical shielding tensors are large, even though the quadrupole interactions are small. Figure 6, a and b, shows typical ^{17}O MASS NMR spectra of solid Mo(bipyr)$(CO)_4$ (bipyr = bipyridine) and K_2WO_4, both enriched to about 20 percent with ^{17}O, which exhibit sharp, multiline spectra. For Mo(bipyr)$(CO)_4$, both *cis* and *trans* CO ligands may be detected, and their shift tensors determined (*49*). For the WO_4^{2-} ion there are three center band peaks together with nine sets of spinning side bands. The isotropic peaks have a 2:1:1 intensity ratio and correspond to the three nonequivalent oxygens observed by means of x-ray crystallography (*50*). Analysis of the side band intensities as a function of spinning rate once again yields the complete chemical-shielding tensors for each nonequivalent oxygen (*8*). However, not all species isoelectronic with WO_4^{2-} have such large shift tensors—indeed, for $KMnO_4$, $\Delta\sigma$ is approximately zero (*8*). Such information will permit more detailed analyses of chemical bonding in polyoxoanions, polyoxocations, and metal carbonyls than before. Already we have shown that the ^{17}O chemical shift is a function of the metal-ion radius for nine MO_4 species isoelectronic with WO_4^{2-} (*8*). These results suggest that observation of ^{17}O shifts in less well defined oxide phases of catalytic interest could give useful information on structure and bonding.

Of more general interest in ^{17}O NMR are the magnitudes of the quadrupole coupling constants and the values of the asymmetry parameters of the electric-field-gradient tensors. For $Mo(CO)_6$ and K_2WO_4, e^2qQ/h values are small, $\simeq$1 MHz; in the case of the carbonyl, this is in part due to π-backbonding, and in the case of the WO_4^{2-} ion, to a fairly weak W–O bond. Indeed, the early x-ray studies were prompted by the idea that the oxygen in such systems might best be regarded as the spherically symmetric O^{2-} species (*50*); that is, the phase was considered a candidate for a mixed-oxide formulation. These systems are clearly not ideal for determining e^2qQ/h values because of the lack of observable quadrupolar structure, although such information may often be deduced with a fair degree of certainty from the field-dependence of the isotropic chemical shift (*42*).

By contrast, the silicate minerals offer a wealth of information, not only about chemical shifts but also about e^2qQ/h and η values. We show in Fig. 6, c and d, the ^{17}O MASS NMR spectra of the olivine mineral forsterite (Mg_2SiO_4) and the pyroxene mineral diopside ($CaMgSi_2O_6$), both enriched to about 20 percent with ^{17}O. Both spectra appear quite complex, but they can be refined into three sets of resonances by means of computer simulations, as shown. For forsterite, there are once again three nonequivalent oxygen sites, as determined by x-ray diffraction (*51*), which give rise to three oxygen resonances with the following e^2qQ/h, η, and σ_i values: O_a (2 oxygens), 2.35 MHz, 0.2, 61.0 ppm; O_b (1 oxygen), 2.35 MHz, 1.0, 62.0 ppm; and O_c (1 oxygen), 2.70 MHz, 0.3, 47.0 ppm (*8*). For diopside, there are also three nonequivalent oxygen sites, two nonbridging and one bridging. We assign the e^2qQ/h, η, and σ_i values as follows: O_{nb}, 2.7 MHz, 0.0, 84 ppm; O_{nb}, 2.8 MHz, 0.2, 63 ppm; and O_{br}, 4.3 MHz, 0.2, 67 ppm. These latter assignments are based on the observation of an intense O_{nb} resonance in the range of 40 to 160 ppm in a variety of pyroxenes, which becomes more deshielded with increasing cation radius, and a weaker O_{br} resonance in the range of 60 to 70 ppm, which does not shift (*52*). Thus, even in quite complex silicate phases, considerable information may be obtained by means of high-field MASS NMR spectroscopy (*8*).

For more covalent species, such as SiO_2, we expect an increase in e^2qQ/h, and indeed, for SiO_2 in the form of low cristobalite we obtain e^2qQ/h = 5.8 MHz, η = 0.1, and σ_i = 36.1 ppm. Even at 11.7 T, the overall breadth of the second-order powder pattern is about 20 kHz, much larger than our highest attainable sample-rotation frequencies (~7 kHz); so it is clearly preferable to utilize variable-angle sample spinning (at 75°) for high-resolution studies of SiO_2 (*8*).

To a first approximation, all of the results we have obtained from ^{17}O NMR may be interpreted in terms of the ionic nature of the bonds between oxygen and its counterions. In Fig. 7a we show e^2qQ/h values plotted as a function of the average ionic nature of the bonds to oxygen, I. As an example, for a silicate containing solely Si–O–Mg bonds, we use Pauling electronegativities to calculate a 51 percent ionic character for the Si–O bond and a 74 percent ionic character for the O–Mg bond, yielding an average of 62.5 percent. Since the data in Fig. 7a may be well fit by a line of the form

$$e^2qQ/h = -0.198\,I + 14.66$$

this equation predicts an e^2qQ/h value for the Si–O–Mg fragment of 2.29 MHz, in good agreement with the 2.47 MHz observed experimentally in forsterite (*8*). This is not unexpected, since similar ideas are employed in Townes-Dailey calculations of e^2qQ/h values, and similar relations have been observed by others in the ^{35}Cl nuclear quadrupole reso-

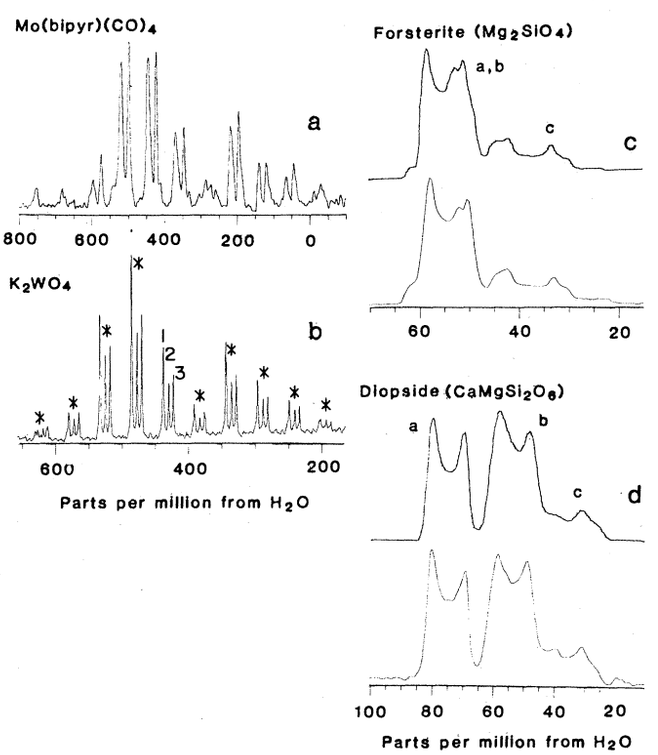

Fig. 6. Oxygen-17 NMR spectra from inorganic solids. (a) MASS NMR spectrum of Mo(bipyr)$(CO)_4$ at 11.7 T showing resolution of *cis* and *trans* carbonyls, large (~700 ppm) chemical shift anisotropy, and small ($\lesssim$1 MHz) quadrupole coupling constant. (b) MASS NMR spectrum of K_2WO_4 at 11.7 T, showing resolution of all three nonequivalent oxygen sites and a large chemical shift anisotropy. (c) MASS NMR spectra of enriched forsterite (Mg_2SiO_4) and diopside ($CaMgSi_2O_6$) at 11.7 T, together with (above) their computer simulations, showing observation of nonequivalent, chemically shifted ^{17}O resonances.

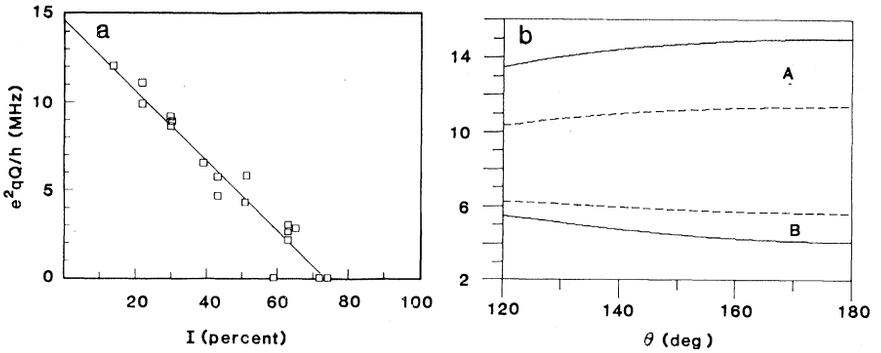

Fig. 7. (a) Oxygen-17 quadrupole coupling constant (e^2qQ/h) plotted as a function of the percent ionic character, I, of the A–O–B bond in a series of oxides and oxyanions. (b) Oxygen-17 e^2qQ/h values plotted as a function of Si–O–Si bond angle, θ, in SiO_2, for bonding schemes involving sigma bonds only (A) and sigma and π-bonds (B).

nance spectra from a series of M–Cl bonds (*53*).

We are now in a position to obtain a wide body of information about the e^2qQ/h and η values for oxygen in geologically and chemically interesting species. It may soon be possible to resolve long-standing questions, such as the degree of π-bonding in silicates (*54–56*).

For example, in Fig. 7b we show the relation between e^2qQ/h and hybridization state (plotted as $Si–O_{br}–Si$ bond angle, θ) for bridging oxygens in the Q^4 silicates. The two lines in case A represent two proposed bonding schemes involving σ orbitals only, whereas the two lines in case B represent π-bonding between oxygen *p*-orbitals and silicon *d*-orbitals (*57*). Clearly, the possible bonding schemes can be differentiated on the basis of e^2qQ/h and η values from ^{17}O spectra. With the availability of more complex computational devices (array processors) and development of appropriate theory, it should also be possible to use ^{17}O (and ^{29}Si) chemical-shift data to facilitate such determinations.

Aluminum-27 NMR Spectra

Aluminum-27 has a nuclear spin I = 5/2 and a quadrupole moment of 0.149×10^{-28} m^2, is 100 percent abundant, and resonates at 130.3 MHz in a magnetic field of 11.7 T. It is thus a most sensitive nucleus and has been investigated extensively in mineral and catalyst systems (*1–5*). Because of this sensitivity, ^{27}Al NMR enables us to carry out a number of studies that would be most difficult with ^{17}O or ^{29}Si, and by way of example we shall discuss three types of experiments.

First, the high sensitivity of ^{27}Al permits the observation of both MASS and static NMR spectra of ^{27}Al nuclei having large e^2qQ/h values. For example, we recently obtained ^{27}Al NMR spectra, both MASS and static, of the basic aluminum-sulfate cluster $Na[AlO_4Al_{12}(OH)_{24}(H_2O)_{12}](SO_4)_4 \cdot \sim 13H_2O$ at 11.7 T and a static spectrum at 8.45 T (360 MHz ^1H-resonance frequency). The aluminum sulfate contains an Al_{13}-polyoxohydroxo cluster with a central AlO_4 unit and 12 octahedral AlO_6 groups (*58*). In the MASS experiment at 11.7 T (*59*), only the central AlO_4 resonance is well resolved, because the absorption from the 12 octahedral aluminums covers about 35 kHz, and a very complex pattern is obtained. At high field, the static spectrum may be recorded with minimal distortion and good sensitivity, but unfortunately, at 11.7 T, the resonance from the single tetrahedral site overlaps one of the singularities of the powder pattern from the 12 octahedral aluminums, and is thus not resolved. By contrast, at 8.45 T there is a substantial second-order shift and an increase in the width of the octahedral aluminum resonance, so both tetrahedral and octahedral sites are clearly seen. Computer simulation of this latter spectrum yields e^2qQ/h and σ_i values for Al(4) of 0.7 MHz and 62.8 ppm, respectively; and for Al(6), of 10.2 MHz and ~8 ppm. The value of η is zero for Al(6) but unknown for Al(4). Although there have been other studies of this compound and related compounds, such information has not been available previously. Analysis of such results are of interest because of the use of these species as models for oxide lattices as well as in personal-care products.

Increased sensitivity also permits the observation of very low concentrations of ^{27}Al—on the order of tens of parts per million. For example, in silicalite, Fyfe *et al.* (*60*) have convincingly demonstrated that during synthesis, aluminum is incorporated into the zeolite lattice (forming the zeolite ZSM-5) rather than being present as adventitious Al_2O_3, as had been claimed previously (*61*), because a characteristic resonance around 55 ppm is observed rather than peaks at about 71 ppm (tetrahedral aluminum) or 9 ppm (octahedral aluminum) as would be expected for the Al_2O_3 polymorphs. Such observations of low aluminum concentrations have considerable promise for the detection of trace aluminum in various minerals. Furthermore, since AlO_6 units in aluminas, aluminates, and aluminosilicates all resonate in the range of about 15 to −20 ppm, whereas AlO_4 units resonate in the range of 80 to 50 ppm, even low aluminum concentrations may be characterized, a difficult task with any other technique.

To date then, the main use of ^{27}Al solid-state NMR, apart from early studies (*62*), has been as an analytical tool for the detection of octahedral and tetrahedral aluminum. Relatively few theoretical interpretations of the NMR data have been published. However, using data from wide-line ^{27}Al NMR at low fields, Ghose and Tsang have attempted to determine some relation for AlO_6 between the quadratic elongation of the octahedron, used as a measure of polyhedral distortion, and e^2qQ/h (*62*). For the Al_{13} aluminum sulfate cluster this treatment yields e^2qQ/h = 10.2 MHz, in good agreement with the NMR experiment, but the relation appears to break down for small values of e^2qQ/h (*59*). Interestingly, in the Al_{13} cluster found in the mineral zunyite, very sharp MASS NMR resonances for both tetrahedral and octahedral Al have been reported (*63*), corresponding to e^2qQ/h values of about 0.6 MHz and 2.5 MHz, respectively. Because the structure of the Al_{13} cluster is essentially the same in the basic sulfate and zunyite, and bond lengths are similar, this suggests that the apparent facial ligand arrangement in zunyite could be the primary cause of the small electric field gradient (*64*). Thus, both the nature and symmetry of the ligand field must always be considered when interpreting e^2qQ/h data. In any case, it is clear that there are considerable opportunities for theoretical developments in interpretation of the e^2qQ/h, η, and σ values for ^{27}Al in inorganic solids now that experimental data may be obtained for numerous materials.

Finally, there has been little rigorous study of the quantitation of quadrupolar signal intensities, especially for aluminum. In some materials—for example, in high-surface-area γ-Al_2O_3 (*65*) and many glasses (*66*)—only a small fraction of the total aluminum present is detected in the MASS NMR experiment. While some

sites may be so distorted as to yield spectral lines that are simply too broad to be observed, especially at low magnetic field strength, other complications can arise because the energy levels with $I = 1/2$ and $-1/2$ are not isolated from the other levels. There may be large spectral intensity changes as a function of the extent to which the various states are excited by the radio-frequency pulse. These effects have been studied (*67*), and they have led to a number of interesting two-dimensional experiments by Samoson and Lippmaa (*67*) that may result in information about quadrupole coupling in the presence of other interactions, such as dipolar broadening. In order to observe sites that are so distorted they are not seen in a conventional pulsed NMR experiment, continuous-wave spectrometers that provide very high fields may be needed. In addition, nuclear quadrupole resonance and "zero-field" NMR (*68*) will likely have great utility.

Spectra from Hydrogen and Other Nuclei

Hydrogen (^{1}H) has a nuclear spin $I = 1/2$, is 99.985 percent abundant, and resonates at 500 MHz in a magnetic field of 11.7 T. It is thus an extremely sensitive nucleus for NMR. However, because of its abundance and large gyromagnetic ratio, the proton-proton dipolar interaction is extremely strong and cannot be removed solely by MASS in, for example, ice, where line widths on the order of 80 kHz are found.

Fortunately, in many technologically interesting materials such as zeolites and some ceramics, the hydrogen content is low, and if the hydrogen is not clustered, relatively narrow lines are expected because the dipole-dipole interaction is inversely proportional to r_{HH}^3, where r_{HH} is the interproton distance. Furthermore, if there is molecular motion present, even further narrowing can occur. This has permitted, for example, the detection of H_2 on Rh-TiO_2 under conditions that give high-resolution spectra (*69*).

Application of MASS NMR to zeolite systems has resulted in high-resolution ^{1}H spectra of solids (*70*), and resonances at 2 and 7 ppm from TMS have been observed for amorphous silica-aluminas. Only the 7 ppm resonance is attributed to catalytically active acidic hydroxyl groups, because the cracking rate of cumene as a function of Al_2O_3 content closely parallels the presence of this spectral feature. In other studies, the dehydroxylation of an HY zeolite has been investigated; as expected, the combination of MASS with a multipulse ^{1}H line-narrowing sequence (*71*) permits the recording of highly resolved ^{1}H spectra, even in the presence of moderate dipolar broadening.

The presence of hydrogen in a sample can also cause line broadening of resonances from other nuclei, and this broadening often cannot be removed by MASS alone. For example, in KH_2PO_4 and the borate mineral inyoite, high-field MASS NMR spectra that are ^{1}H-coupled are essentially featureless, and little information can be extracted (*72*). By contrast, in the presence of a strong ^{1}H radio-frequency field (at 500 MHz) during ^{11}B or ^{31}P data acquisition, the effects of ^{1}H dipolar coupling are eliminated, and high-resolution spectra are obtained. In the case of the ^{11}B spectrum from inyoite, spectral simulation reveals the expected 1:2 ratio between trigonal boron ($e^2qQ/h = 2.4$ MHz, $\eta = 0.0$, $\sigma_i = 19.4$ ppm) and tetrahedral boron ($e^2qQ/h \approx 0$ MHz, $\sigma_i = 2.3$ ppm); whereas for the ^{31}P spectrum of KH_2PO_4, analysis of the side band intensities as a function of spinning rate yields the elements of the chemical-shift tensor (*72*).

An application of solid-state ^{31}P NMR is the structural study of the mineral phases of bone as a function of maturation. For example, Herzfeld *et al.* (*73*) confirmed by NMR that low-density bone is composed primarily of brushite ($CaHPO_4 \cdot 2H_2O$) while high-density bone is mainly hydroxyapatite [$Ca_{10}(PO_4)_6(OH)_2$], which had been known from x-ray work (*74*). However, they also found that whole mid-diaphysis tibiae in 17-day-old chick embryos appear to be composed of a mixture of brushite and apatite in a 1:2 ratio. In this case x-ray diffraction detected only apatite (*73*), presumably because the brushite crystallites were exceedingly small and could well be distorted. Related studies have been performed with dental materials (*75*), and this technique offers promise for the definitive characterization of amorphous or heterogeneous phases where x-ray techniques fail.

The results presented in this and the preceding sections indicate that most of the main group elements in the periodic table are now accessible to study with high-field, rapid-sample-spinning NMR techniques. Although there have been few reports to date, many heavy-metal nuclei with very low sensitivities, such as ^{103}Rh, ^{109}Ag, and ^{183}W, should also be accessible when cross-polarization techniques (*76, 77*) are used to transfer magnetization from abundant ^{1}H nuclei to the rarer species with low-sensitivity. Detailed analysis of the dynamics of such experiments should provide much useful information on bond lengths and dynamics in solids, which should be of considerable utility in probing the nature of various species bound to catalyst surfaces (*78, 79*).

The results we have presented above indicate that new areas of research in the earth sciences, in the materials sciences, and in inorganic chemistry are becoming available through advances in NMR spectroscopy. Given the impact that high-resolution NMR of solutions has had in many areas of chemistry over the past 20 years, we believe that a similar impact can be predicted for the NMR of inorganic solids.

References and Notes

1. E. Lippmaa, M. Mägi, A. Samoson, G. Engelhardt, A.-R. Grimmer, *J. Am. Chem. Soc.* **102**, 4889 (1980).
2. C. A. Fyfe, J. M. Thomas, J. Klinowski, G. C. Gobbi, *Angew. Chem. Int. Ed. Engl.* **22**, 159 (1983).
3. E. Lippmaa, M. Mägi, A. Samoson, M. Tarmak, G. Engelhardt. *J. Am. Chem. Soc.* **103**, 4992 (1981).
4. D. Müller, W. Gessner, H.-J. Behrens, G. Scheler, *Chem. Phys. Lett.* **79**, 59 (1981).
5. M. D. Meadows, K. A. Smith, R. A. Kinsey, T. W. Rothgeb, R. P. Skarjune, E. Oldfield, *Proc. Natl. Acad. Sci. U.S.A.* **79**, 1351 (1982).
6. S. Ganapathy, S. Schramm, E. Oldfield, *J. Chem. Phys.* **77**, 4360 (1982).
7. S. Schramm, R. J. Kirkpatrick, E. Oldfield, *J. Am. Chem. Soc.* **105**, 2483 (1983).
8. S. Schramm and E. Oldfield, *ibid.* **106**, 2502 (1984).
9. E. R. Andrew, A. Bradbury, R. G. Eades, *Nature (London)* **183**, 1802 (1959).
10. I. J. Lowe, *Phys. Rev. Lett.* **2**, 285 (1959).
11. E. R. Andrew, in *Progress in Nuclear Magnetic Resonance Spectroscopy*, J. W. Emsley, J. Feeney, L. H. Sutcliffe, Eds. (Pergamon, New York, 1971).
12. A. C. Cunningham and S. M. Day, *Phys. Rev.* **152**, 287 (1966); A. Tzalmona and E. R. Andrew, *Proc. Colloq. AMPERE At. Mol. Etud. Radio Elec.* **18**, 241 (1974).
13. E. R. Andrew, M. Firth, A. Jasinski, P. J. Randall, *Phys. Lett. A* **31**, 446 (1970).
14. E. Lippmaa, M. Alla, T. Tuherm, *Proc. Colloq. AMPERE At. Mol. Etud. Radio Elec.* **19**, 113 (1976).
15. E. R. Andrew, W. S. Hinshaw, R. S. Tiffen, *J. Magn. Reson.* **15**, 191 (1974).
16. J. S. Waugh, M. M. Maricq, R. Cantor, *ibid.* **29**, 183 (1978).
17. G. R. Holzman, P. C. Lauterbur, J. H. Anderson, W. Koth, *J. Chem. Phys.* **25**, 172 (1956).
18. J. R. Clark *et al.*, *Mineral. Soc. Amer. Spec. Pap.* **2**, 33 (1969).
19. Y. Ohashi and L. W. Finger, *Carnegie Inst. Washington Yearb.* **75**, 743 (1976).
20. K. A. Smith, R. J. Kirkpatrick, E. Oldfield, D. M. Henderson, *Am. Mineral.* **68**, 1206 (1983).
21. M. T. Melchior, D. E. W. Vaughan, R. H. Jarman, A. J. Jacobson, *Nature (London)* **298**, 455 (1982).
22. W. Loewenstein, *Am. Mineral.* **39**, 92 (1954).
23. J. Klinowski, S. Ramdas, J. M. Thomas, C. Fyfe, J. S. Hartman, *J. Chem. Soc. Faraday Trans. 2* **78**, 1025 (1982); G. Engelhardt, U. Lohse, A. Samoson, M. Mägi, M. Tarmak, E. Lippmaa, *Zeolites* **2**, 59 (1982).
24. W.-H. Yang, R. J. Kirkpatrick, M. Vergo, M. McHone, T. I. Emilsson, E. Oldfield, in preparation.
25. J. M. Thomas, J. Klinowsky, S. Ramdas, M. W. Anderson, G. A. Fyfe, G. C. Gobbi, *ACS Symp. Ser.* **218**, 159 (1983).
26. I. D. Brown and R. D. Shannon, *Acta Crystallogr. Sect. A* **29**, 266 (1973).
27. K. A. Smith, R. J. Kirkpatrick, D. M. Henderson, E. Oldfield, in preparation; M. Mägi, E. Lippmaa, A. Samoson, G. Engelhardt, A.-R. Grimmer, *J. Phys. Chem.* **88**, 1518 (1984).
28. W. H. Baur, *Acta Crystallogr. Sect. B* **34**, 1751 (1978).

29. W. D. Kingery, H. K. Bowen, D. R. Ullman, *Introduction to Ceramics* (Wiley, New York, 1976).
30. J. V. Smith and C. S. Blackwell, *Nature (London)* **303**, 223 (1983).
31. _____, G. L. Hovis, *ibid.* **309**, 140 (1984).
32. G. V. Gibbs, *Am. Mineral.* **67**, 421 (1982).
33. S. Ramdas and J. Klinowski, *Nature (London)* **308**, 521 (1984).
34. E. Dupree and R. F. Pettifer, *ibid.*, p. 523.
35. E. Oldfield, R. A. Kinsey, B. Montez, T. Ray, K. A. Smith, *J. Chem. Soc. Chem. Commun.* (1982), p. 254.
36. J. Herzfeld and A. E. Berger, *J. Chem. Phys.* **73**, 6021 (1980).
37. E. R. Andrew, *Arch. Sci. Genève* **12**, 103 (1959).
38. A. Nolle, *Z. Phys. A* **280**, 231 (1977).
39. H.-J. Behrens and B. Schnabel, *Physica B* **114**, 185 (1982).
40. A. Vega, private communication.
41. E. Oldfield *et al.*, *J. Am. Chem. Soc.* **104**, 919 (1982).
42. D. Müller, J. Grunze, E. Hallas, G. Ladwig, *Z. Anorg. Allg. Chem.* **500**, 80 (1983).
43. A. Samoson, E. Kundla, E. Lippmaa, *J. Magn. Reson.* **49**, 350 (1982).
44. S. Schramm and E. Oldfield, *J. Chem. Soc. Chem. Commun.* (1982), p. 980.
45. M. A. Fedotov and G. F. Gerasimova, *React. Kinet. Catal. Lett.* **22**, 113 (1983).
46. G. E. Maciel, B. L. Hawkins, J. S. Frye, C. E. Bronnimann, paper presented at the 25th Experimental NMR Conference, Wilmington, Del., April 1984.
47. G. L. Turner, S. E. Chong, E. Oldfield, in preparation.
48. R. E. J. Sears, *J. Chem. Phys.* **61**, 4368 (1974).
49. E. Oldfield, M. A. Keniry, S. Schramm, S. Shinoda, H. S. Gutowsky, T. L. Brown, in preparation.
50. A. S. Koster, F. X. N. M. Kools, G. D. Rieck, *Acta Crystallogr. Sect. B* **25**, 1704 (1969).
51. G. E. Brown, in *Reviews in Mineralogy*, P. H. Ribbe, Ed. (Mineral Society of America, Washington, D.C., 1982), vol. 5, p. 275.
52. S. Schramm, R. J. Kirkpatrick, E. Oldfield, unpublished results.
53. L. Ramakrishnan, S. Soundararajan, V. S. S. Sastry, J. Ramakrishna, *Coord. Chem. Rev.* **22**, 123 (1977).
54. R. F. Stewart, M. A. Whitehead, G. Donnay, *Am. Mineral.* **65**, 324 (1980).
55. L. Pauling, *ibid.*, p. 321.
56. D. W. J. Cruickshank, *J. Chem. Soc. London* **1077**, 5486 (1961).
57. N. Janes and E. Oldfield, in preparation.
58. G. Johansson, *Acta Chem. Scand.* **16**, 403 (1962).
59. A. C. Kunwar, A. Thompson, H. S. Gutowsky, E. Oldfield, in preparation.
60. C. A. Fyfe, G. C. Gobbi, J. Klinowski, J. M. Thomas, S. Ramdas, *Nature (London)* **296**, 530 (1982).
61. E. M. Flanigen *et al.*, *ibid.* **271**, 512 (1978).
62. S. Ghose and T. Tsang, *Am. Mineral.* **58**, 748 (1973).
63. F. v. Lampe. D. Müller, W. Gessner, A.-R. Grimmer, G. Scheler, *Z. Anorg. Allg. Chem.* **489**, 16 (1982).
64. K. A. Valiev and M. M. Zaripov, *Zh. Strukt. Khim.* **7**, 494 (1966); V. P. Tarasov, V. I. Privalov, Yu. A. Buslaev, *Mol. Phys.* **35**, 1047 (1978).
65. V. M. Mastikhin, O. P. Krivoruchko, B. P. Zolotovskii, R. A. Buyanov, *React. Kinet. Catal. Lett.* **18**, 117 (1981).
66. B. M. W. S. deJong, C. M. Schramm, V. E. Parziale, *Geochim. Cosmochim. Acta* **47**, 1223 (1983).
67. V. H. Schmidt, *Proc. Ampère Intl. Summer School II*, 75 (1971); A. Samoson and E. Lippmaa, *Phys. Rev. B* **28**, 6567 (1983); *Chem. Phys. Lett.* **100**, 205 (1983).
68. D. P. Weitekamp, A. Bielecki, D. Zax, K. Zilm, A. Pines, *Phys. Rev. Lett.* **50**, 1807 (1983); A. Bielecki *et al.*, *J. Chem. Phys.* **80**, 2232 (1984).
69. P. Gajardo, T. M. Apple, C. Dybowski, *Chem. Phys. Lett.* **74**, 306 (1980).
70. D. Freude, M. Hunger, H. Pfeifer, *ibid.* **91**, 307 (1982); M. Hunger, D. Freude, H. Pfeifer, H. Bremer, M. Jank, K. P. Wendlandt, *ibid.* **100**, 29 (1983).
71. J. S. Waugh, L. M. Huber, U. Haeberlen, *Phys. Rev. Lett.* **20**, 180 (1968).
72. G. L. Turner, K. A. Smith, R. J. Kirkpatrick, E. Oldfield, in preparation.
73. J. Herzfeld, A. Roufosse, R. A. Haberkorn, R. G. Griffin, M. J. Glimcher, *Philos. Trans. R. Soc. London Ser. B* **289**, 459 (1980).
74. M. J. Glimcher, in *Handbook of Physiology, Endocrinology*, R. O. Greep and E. B. Astwood, Eds. (American Physiological Society, Washington, D.C., 1976), vol. 7, p. 25; A. Roufosse, W. J. Landis, W. K. Sabine, M. J. Glimcher, *J. Ultrastruct. Res.* **68**, 235 (1979).
75. W. P. Rothwell, J. S. Waugh, J. P. Yesinowski, *J. Am. Chem. Soc.* **102**, 2637 (1980).
76. A. Pines, M. G. Gibby, J. S. Waugh, *J. Chem. Phys.* **56**, 1776 (1972).
77. B. L. Hawkins, A. Bax, G. E. Maciel, paper presented at the 25th Experimental NMR Conference, Wilmington, Del., 1984.
78. E. Oldfield, T. L. Brown, M. A. Keniry, S. Schramm, S. Shinoda, paper presented at the 24th Experimental NMR Conference, Asilomar, Calif., 1983; B. E. Hanson, G. W. Wagner, R. J. Davis, E. Motell, *Inorg. Chem.* **23**, 1636 (1984).
79. C. D. Makowa, C. P. Slichter, J. H. Sinfelt, *Phys. Rev. Lett.* **49**, 379 (1982).
80. We thank the members of our research groups, especially S. E. Schramm, K. A. Smith, V. Jacob, and E. Chong, for their assistance in preparing this article. Supported by National Science Foundation (NSF) grants DMR-8311339 and EAR 8207260. Use of equipment provided by NSF grants CHE 7916100, EAR 8218741, and PCM 8306283 is also acknowledged.

Promoting Functional Plasticity in the Damaged Nervous System

William J. Freed, Luis de Medinaceli, Richard Jed Wyatt

Not long ago it was commonly believed that the adult mammalian central nervous system (CNS) was structurally static—that severed neurites did not regrow and functionally significant structural adjustments did not occur. When recovery of function following brain lesions was observed it was attributed to the brain's capacity to circumvent the lesion by mechanisms such as denervation supersensitivity or the use of alternative pathways (*1*). In contrast, peripheral nerves were known to regenerate after being injured, sometimes with recovery of function (*2, 3*). The consequence of this pessimistic view was that scientific interest in neuronal plasticity was mainly directed at lower animals, immature systems, and peripheral nerves.

Terminal fields vacated as a consequence of CNS injury are commonly filled by the growth of axon collaterals, or collateral sprouting (*4*). Neuronal plasticity, and collateral sprouting in particular, now appears to be a ubiquitous phenomenon in the mature CNS that can have functional consequences (*5, 6*). A considerable body of information pertaining to the cellular biology of collateral sprouting and synaptic plasticity now exists (*7*). Here we discuss neuronal plasticity from the perspective of functional restitution; that is: Can neuronal plasticity be manipulated or exploited to obtain functional benefits?

The authors are scientists in the Preclinical Neurosciences Section, Neuropsychiatry Branch, National Institute of Mental Health, St. Elizabeths Hospital, Washington, D.C. 20032.

Axonal Plasticity in the Normal Nervous System

In the peripheral nervous system, severed neurites invariably regenerate. So vigorous is this regeneration that it persists in the stump even after removal of a limb, resulting in the formation of a neuroma (*2, 3*). As peripheral neurites grow, contact with Schwann cells stimulates myelination and some formation of new or additional basal lamina (*8–10*).

In the mature mammalian CNS, myelinated tracts, including those of the spinal cord, are unable to regenerate through the site of a lesion (*11, 12*). Certain categories of unmyelinated or thinly myelinated CNS neurites show substantial regeneration provided no physical barrier is produced when they are damaged (*13*).

Scarring at the site of a CNS lesion is greatly reduced in the immature animal; nonetheless, most studies agree that immature neurites cannot penetrate a CNS lesion to any greater degree than those of a mature animal (*14*). In most cases where regeneration is observed in either immature or adult animals, it occurs around, rather than through, the lesion site (*11, 15–17*). For example, function is spared after pyramidal and corticospinal tract lesions in infant animals (*15, 16*). The anatomical basis of this sparing is probably either a regrowth of late-devel-